Single-Ion Magnetic Anisotropy and Isotropic Magnetic Couplings in the Metal−Organic Framework Fe₂(dobdc)

Rémi Maurice,[†] Pragya Verma,[†] Joseph M. Zadrozny,[‡] Sijie Luo,[†] Joshua Borycz,[†] Jeffrey R. Long,*[,‡] Donald G. Truhlar,*[,†] and Laura Gagliardi*[,†]

[†]Department of Chemistry, Supercomputing Institute, and Chemical Theory Center, University of Minnesota, Minneapolis, Minnesota 55455, United States

[‡]Department of Chemistry, University of California, Berkeley, California 94720, United States

Ⓢ Supporting Information

ABSTRACT: The metal−organic framework Fe₂(dobdc) (dobdc⁴⁻ = 2,5-dioxido-1,4-benzenedicarboxylate), often referred to as Fe-MOF-74, possesses many interesting properties such as a high selectivity in olefin/paraffin separations. This compound contains open-shell Fe^{II} ions with open coordination sites which may have large single-ion magnetic anisotropies, as well as isotropic couplings between the nearest and next nearest neighbor magnetic sites. To complement a previous analysis of experimental data made by considering only isotropic couplings [Bloch et al. *Science* **2012**, *335*, 1606], the magnitude of the main magnetic interactions are here assessed with quantum chemical calculations performed on a finite size cluster. It is shown that the single-ion anisotropy is governed by same-spin spin−orbit interactions (i.e., weak crystal-field regime), and that this effect is not negligible compared to the nearest neighbor isotropic couplings. Additional magnetic data reveal a metamagnetic behavior at low temperature. This effect can be attributed to various microscopic interactions, and the most probable scenarios are discussed.
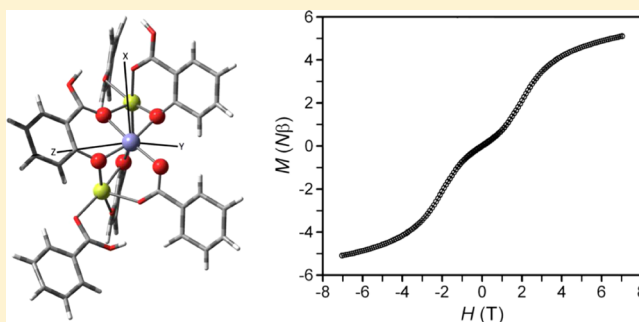
1. INTRODUCTION

Transition metal based nanoporous materials are attracting the attention of many scientists because of their high selectivity in gas separations,[1−6] catalytic activity,[7,8] and magnetic properties.[9−13] Many of their properties are linked to the presence of open-site transition metal ions, which may have open shells depending on their d^n configuration and their coordination environments inside the framework. If the metal ions are connected by organic linkers, one may refer to such materials as metal−organic frameworks (MOFs), coordination polymers, or coordination networks.

Among this newly popular class of materials, the Fe₂(dobdc) (dobdc⁴⁻ = 2,5-dioxido-1,4-benzenedicarboxylate) system, referred to as Fe-MOF-74, is particularly noteworthy. It exhibits very high performance for the separation of methane/ethane/ethylene/acetylene mixtures[2,14,15] and can selectively bind O₂ over N₂.[16] The structure of this compound consists of high-spin Fe^{II} ions arranged in a helical pattern along columns at the intersection of three hexagonal pores. As synthesized, each Fe^{II} ion is hexacoordinate; five coordination sites occupied by dobdc⁴⁻ ligands and one by solvent. Upon activation, however, the coordinating solvent is removed, leaving the Fe^{II} ion in a pentacoordinate environment. The first coordination sphere around each Fe^{II} ion is a distorted square pyramid (SPy), with the oxygen atoms of the dobdc⁴⁻

ligands bridging to other Fe^{II} ions along the same or other helical chains (see Figure 1).

A detailed analysis of the magnetic properties of Fe₂(dobdc) by the spin Hamiltonian approach can be problematic. The universal starting point of representing the system by a phenomenological spin Hamiltonian[17] involves exchange integrals J_{ab} and effective local spins $\hat{S}_a$, sometimes called fictitious spins.[18] These exchange integrals, which describe the interactions of spins on magnetic centers a and b, are called isotropic magnetic couplings. Interactions can also occur between spins on the same metal center because of ligand field and spin−orbit interactions. These intra-ion interactions are usually described by the effective second-order perturbation theory parameters D and E, which correspond to the axial and rhombic zero-field splitting parameters, respectively.[18] As given, this picture of the magnetic interactions is simple, yet it is nearly impossible to simultaneously extract the magnitudes of all the spin Hamiltonian parameters present in a system (i.e., J_{ab}, D, and E) from one measurement technique without approaching overparameterization. A previous analysis of the magnetic susceptibility data of Fe₂(dobdc) attempted to avoid the overparameterization problem by using a model that only included inter- and intrachain isotropic magnetic couplings.[2]
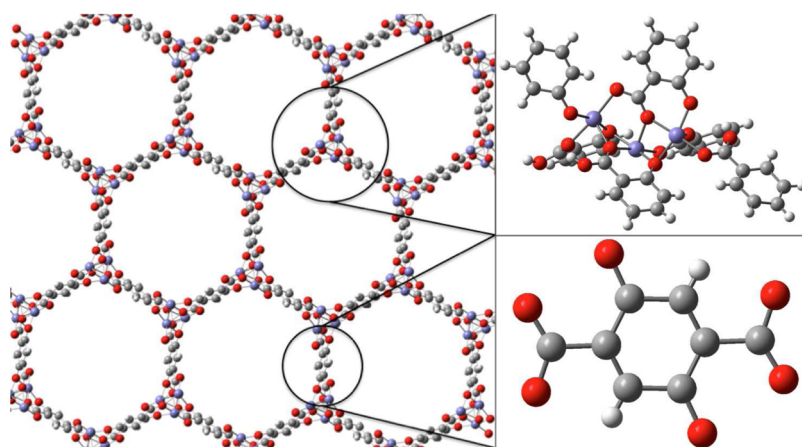
Figure 1. Crystal structure of Fe_2(dobdc) (dobdc^{4-} = 2,5-dioxido-1,4-benzenedicarboxylate) (left), structure of the 88-atom cluster used for computation (top right) and of the dobdc^{4-} ligand (bottom right), where Fe atoms are represented in purple, O atoms in red, C atoms in dark gray, and H atoms in light gray.

Note that, though the quality of the fit was good, the model did not address the probability that the Fe^{II} spin centers are appreciably anisotropic. Recent work has demonstrated that coordinatively saturated and unsaturated Fe^{II} ions can possess very large magnetic anisotropies.[19−23] Furthermore, the previous analysis did not account for intrachain next-nearest neighbor interactions, which can in some systems compete with nearest neighbor interactions[24,25] and lead to spiral spin orderings (and we note that some omitted intrachain interactions involve Fe atoms closer than those involved in the included interchain interactions). Here we revisit this problem via quantum mechanical electronic structure calculations. We use a cluster approach, and effective interactions are addressed by choosing a given level of electronic structure theory and basis set and by selecting the ions to be explicitly treated. For instance, the calculation of the single-ion anisotropy parameters requires one to treat explicitly (at least) one magnetic center, while the calculation of isotropic magnetic couplings requires at least two. With these considerations in mind, the choice of clusters is not unique, and one has to catch in them the most important electronic effects present in the real material. Note that the isotropic interactions addressed in the present work have been obtained from periodic calculations by Canepa et al.[26]

Several methods are now available for the computation of single-ion anisotropies, based on both density functional theory (DFT)[27−31] and wave function theory (WFT).[32−36] The interpretation and analysis of magnetic data of transition metal complexes is a very active field, and computational and theoretical studies can play a useful role in interpreting experiments.[37−41] With these methods, valuable information can be obtained on the anisotropy of metal ions even in non-standard coordination environments, for example, distorted pentacoordinate and heptacoordinate environments.[42−44] In cases closer to ideal geometries, the results of quantum chemical calculations can also be connected to crystal-field theory to gain further insights into the factors governing the anisotropy.[45−49] Since MOFs can present transition metal ions in unprecedented coordination environments, the theoretical determination of the single-ion anisotropies is particularly important. Part of the present paper is therefore devoted to the determination of the single-ion anisotropy in Fe_2(dobdc), which is expected to be large, as in mononuclear

heptacoordinate Fe^{II} complexes.[21,43] Indeed, in a ligand field picture, both situations show near degeneracy of orbital configurations that can be coupled via the spin−orbit operator once the spin is introduced, resulting in large zero-field splittings. In many cases, WFT approaches have led to single-ion anisotropic parameters in good agreement with experimental values,[29,34,36,40,42,43] and sometimes in better agreement than those obtained by DFT.[32,50,51] Therefore, we will use WFT to predict the values of the single-ion magnetic anisotropy parameters in Fe_2(dobdc).

Isotropic magnetic couplings can be extracted from computed energies of spin-adapted wavefunctions or broken-spin-symmetry solutions, which can be obtained from either WFT or DFT calculations.[52] Within the cluster approach, a wide choice of methods based on WFT and/or DFT is available. WFT studies usually involve a complete active space self-consistent field (CASSCF) calculation where the active space includes the magnetic electrons and orbitals, followed by a perturbative and/or variational treatment of the most important remaining electron correlation effects. As shown in a series of papers by Calzado et al.,[53−55] a careful treatment of the dynamic correlation is required to obtain accurate couplings; in particular, in a WFT approach, all the excited determinants contributing to the magnetic coupling at second order of perturbation have to be treated variationally. This leads to very expensive multi-reference configuration interaction (MRCI) calculations, which become impractical when several magnetic centers are considered. Alternatively, DFT studies only require the treatment of single Slater determinants, but the results may be strongly dependent on the exchange-correlation functional. It is therefore necessary to check the accuracy of the functionals to treat magnetic couplings. We note, however, that newly developed functionals appear to be particularly accurate,[56,57] thus simplifying the process of functional selection. Given this fact, and the relative computational ease with respect to WFT methods, we chose DFT as the preferred method for determination of the isotropic coupling constants for Fe_2(dobdc).

Herein, we present a detailed theoretical and experimental analysis of the single-ion magnetic anisotropy and isotropic magnetic couplings in Fe_2(dobdc). The choice of the cluster will be described, as well as the phenomenological Hamiltonians, the computational details, and information concerning

the extraction of the relevant effective parameters. Then, results for the single-ion anisotropy and magnetic couplings will be presented, as well as additional magnetic data analysis, followed by a discussion.

2. MAGNETIC MEASUREMENTS

Fe_2(dobdc) was prepared according to the published procedures.[16] All handling of the compound during sample preparation was performed under an inert atmosphere. Powdered samples of Fe_2(dobdc) were restrained with a plug of glass wool within a sealed quartz tube for measurement. Magnetic data were collected using a Quantum Design MPMS−XL SQUID magnetometer at temperatures from 1.8 to 300 K and applied direct current (DC) fields from 0 to 7 T. Alternating current (AC) susceptibility measurements were performed with a 4 Oe applied switching field. No effects of crystallite torquing were observed during any measurement. AC and DC magnetic susceptibility data were corrected for diamagnetic contributions from the sample holder and glass wool, as well as for the core diamagnetism of each sample (estimated using Pascal's constants).[58]

3. THEORETICAL AND COMPUTATIONAL STUDY

3.1. Description of the System. *3.1.1. Model for the Isotropic Coupling Calculations.* The isotropic magnetic couplings are calculated for an 88-atom model[59] of Fe_2(dobdc) (as shown in Figure 2) that contains three pentacoordinate Fe^{II} centers and six organic
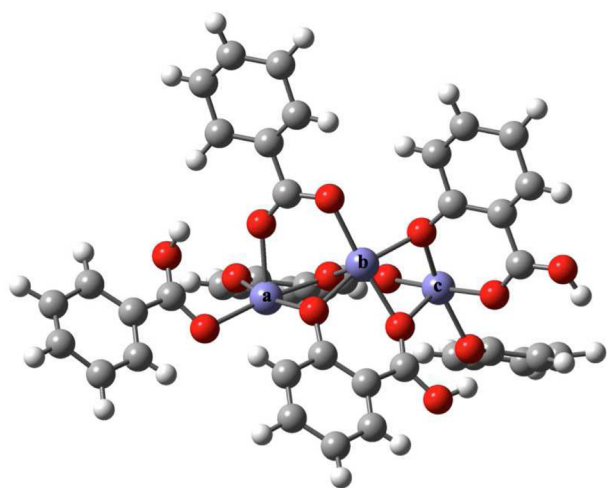
Figure 2. Eighty-eight atom model of Fe_2(dobdc) designed from its crystal structure as viewed along an axis perpendicular to the *c* axis, which is the axis through the helical column of Fe atoms. The three iron ions within the structure are labeled as a, b, and c from left to right. The Fe atoms are represented in purple, O atoms in red, C atoms in dark gray, and H atoms in light gray.

linkers. Four of the six organic linkers coordinate the central iron ion, and the 88-atom cluster has been designed in such a way that the overall charge on the model is zero and the first coordination sphere of

the central iron ion is unmodified from the crystal, whereas the structural features farther away from the central iron ion are truncated to terminate the cluster. Note that the charge of the model has been set to zero by a judicious addition of protons. In the extended structure, all Fe^{II} centers are symmetry equivalent; however, in our truncated model cluster, for which we have ensured a neutral charge, they have slightly different coordination environments. We assume that the Madelung field does not affect significantly the computed energy differences, that is, it is expected to have a minor effect on these energy differences compared to the local bonding, electrostatic, and correlation effects that are explicitly treated in the 88-atom model.

Each of the Fe^{II} centers is in a high spin state ($S = 2$, $M_S = 2$). For the purpose of calculating isotropic coupling constants between the three iron centers, a value of M_S of either 2 or −2 is assigned to each of the iron centers. We have considered four possible ways to assign these M_S values ("spin states") in the four Slater determinants studied using density functional calculations. In the first case, a local spin component of 2 is assigned to all the three iron centers, labeled *a*, *b*, and *c* in Figure 2, making the total spin of the model equal to $S = 6$. In the second case, a local spin component of 2 is assigned to both the leftmost and the central iron centers (*a* and *b*, respectively) and a −2 spin component is assigned to the rightmost iron center (*c*) leading to the overall spin component of the model being $M_S = 2$. In the third case, both the peripheral iron centers (*a* and *c*) are assigned a local spin component of 2 while the central iron ion has a local spin component of −2 which also results in the total spin of the model being $M_S = 2$. In the fourth case, a local spin component of −2 is assigned to the leftmost iron center (*a*) and a spin component of 2 to the central and the rightmost iron centers (*b* and *c*, respectively) leading to the overall spin component of the model being $M_S = 2$. Although the Slater determinants of the second through fourth states do not correspond to a definite value of the spin quantum number S, these four states can be used in a straightforward way for calculating the coupling constants. All four possibilities are shown schematically in Figure 3.

3.1.2. Model for the Single-Ion Anisotropy Calculations. The single-ion anisotropy arises from the joint effects of the ligand field and spin−orbit coupling (SOC); these effects are mainly determined by the metal center and its first coordination sphere. Note, however, that the extreme sensitivity of the magnetic anisotropy of transition metal ions to their surroundings leads to a significant influence upon *D* from metal ions immediately outside the first coordination sphere.[40,60] Hence, we also include the effect of the two nearest-neighbor Fe^{II} ions, and more specifically their influence on the crystal field felt by the central one. Since an explicit treatment of these additional Fe^{II} ions would dramatically complicate the analysis, we model them in the anisotropy calculations by closed-shell ions with the same nominal charge and a similar ionic radius, in particular by Zn^{II} ions. The cluster considered for these calculations is the 88-atom cluster described previously[59] and above, where two of the three Fe^{II} ions, in particular the peripherical ones, have been replaced by Zn^{II} ions, while all the atomic positions remain the same.

3.2. Phenomenological Hamiltonians. In general permanent magnetization in a system like Fe_2(dobdc) can be caused in three possible ways:[18,61−63] (i) ferromagnetic exchange interactions of directly interacting metal ions or superexchange of metal ions by
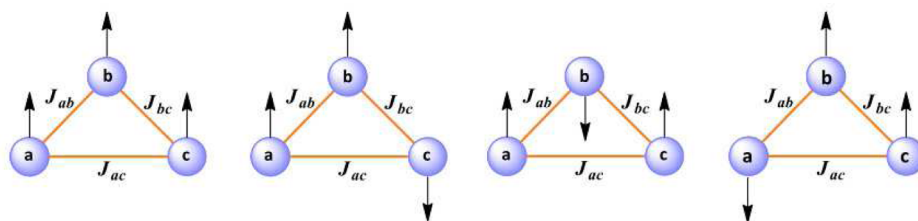
Figure 3. Schematic representation of all four cases of spin states considered on the three iron centers of the 88-atom model. The arrows denote the direction of the local spins at the quintet Fe^{II} centers.

bridging ligands within a chain of iron ions, (ii) single-ion anisotropy because of lower than cubic symmetry at the spin center, or (iii) magnetic dipole coupling between the one-dimensional chains of iron ions. The third contribution is typically the least important although it could become important at low temperature. Nevertheless the present article considers only (i) and (ii).

In keeping with the previous paragraph, we employ two phenomenological Hamiltonians, one to determine the single-ion magnetic anisotropy parameters and one to model the exchange and superexchange coupling of magnetic sites along the chains of iron ions.

3.2.1. Single-Ion Hamiltonian. The effective Hamiltonian operator for single-ion anisotropy is sometimes called the zero-field splitting (ZFS) Hamiltonian or the fine structure Hamiltonian. It is given by[18,34,47,64−67]

$$\hat{H}_{ZFS} = \hat{\mathbf{S}}_b \cdot \mathbf{D} \cdot \hat{\mathbf{S}}_b \tag{1}$$

where $\hat{\mathbf{S}}_b$ is the vector operator for the effective spin of center b, and $\mathbf{D}$ is the second-order anisotropy tensor. The coordinate system that diagonalizes $\mathbf{D}$ is called the magnetic axis frame. In this frame, the Hamiltonian becomes

$$\hat{H}_{ZFS} = D\hat{S}_z^2 + E(\hat{S}_x^2 - \hat{S}_y^2) \tag{2}$$

where z is the highest-symmetry axis, and

$$D = D_{zz} - \frac{1}{2}(D_{xx} + D_{yy}) \tag{3}$$

and

$$E = \frac{1}{2}(D_{xx} - D_{yy}) \tag{4}$$

$\hat{H}_{ZFS}$ splits the states of the ion when $S > 1/2$. The parameter D is called the axial ZFS parameter because E, which is called the rhombic ZFS parameter, vanishes for a system with a 3-fold or higher axis of symmetry. D is nonzero only if the symmetry is less than cubic or octahedral. D may have either sign, but E is here chosen positive by convention, and $E/|D|$ ranges from 0 (the "axial limit") to 1/3 (the "rhombic limit"). Negative D is necessary for the magnetic bistability associated with single-molecule magnets.[68] When D is negative, z is the "easy axis" of magnetization. Note that the D and E parameters have units of energy.

Both first-order spin−spin interactions and second-order spin−orbit coupling (SOC) contribute to the anisotropy; for transition metals the latter usually dominates.[18,68] Several studies concerning single-ion anisotropy[29,50,69,70] or intersite magnetic anisotropy[71] showed that the first-order spin−spin contribution becomes non-negligible in the case of small to moderate zero field splitting. When the SOC contribution to the anisotropy is large, however, the spin−spin interactions become negligible. As we will show later, this situation occurs in $Fe_2(dobdc)$, and therefore only SOC is included in the present study. We will calculate the phenomenological parameters D and E by carrying out electronic structure calculations including SOC (as explained in Section 3.3.1) and calculating the parameters either directly by second-order perturbation theory or, for higher accuracy, by fitting variationally calculated energy levels to eq 2.

The representation of eq 1 in the magnetic axis frame is given in Table 1. The eigenvalues and eigenvectors[29,72] of this matrix are given in Table 2. The eigenvalue expressions in Table 2 are independent of

Table 1. Matrix of the Single-Ion Model Hamiltonian in the $|S_b, M_S(b)\rangle$ Basis in the Magnetic Axis Frame

$\hat{H}_{mod}$	$\lvert 2,-2\rangle$	$\lvert 2,-1\rangle$	$\lvert 2,0\rangle$	$\lvert 2,1\rangle$	$\lvert 2,2\rangle$
$\langle 2,-2\rvert$	$4D$	0	$\sqrt{6}E$	0	0
$\langle 2,-1\rvert$	0	D	0	$3E$	0
$\langle 2,0\rvert$	$\sqrt{6}E$	0	0	0	$\sqrt{6}E$
$\langle 2,1\rvert$	0	$3E$	0	D	0
$\langle 2,2\rvert$	0	0	$\sqrt{6}E$	0	$4D$

the sign of D, but we have listed the states in order of increasing energy for the case where D is negative.

Table 2. Eigenvalues and Eigenvectors of the Single-Ion Model Hamiltonian of Table 1

model state	model energy	model vector[a]
ϕ_1	$2D - 2\sqrt{D^2 + 3E^2}$	$\frac{c_1}{\sqrt{2}}\{\lvert 2,2\rangle + \lvert 2,-2\rangle\} - c_2\lvert 2,0\rangle$
ϕ_2	$4D$	$\frac{1}{\sqrt{2}}\{\lvert 2,2\rangle - \lvert 2,-2\rangle\}$
ϕ_3	$D - 3E$	$\frac{1}{\sqrt{2}}\{\lvert 2,1\rangle - \lvert 2,-1\rangle\}$
ϕ_4	$D + 3E$	$\frac{1}{\sqrt{2}}\{\lvert 2,1\rangle + \lvert 2,-1\rangle\}$
ϕ_5	$2D + 2\sqrt{D^2 + 3E^2}$	$\frac{c_2}{\sqrt{2}}\{\lvert 2,2\rangle + \lvert 2,-2\rangle\} + c_1\lvert 2,0\rangle$

[a] c_1 and c_2 are functions of the D and E parameters.

3.2.2. Spin Coupling Hamiltonian. The coupling of magnetic sites by exchange interactions is represented by the Heisenberg−Dirac−Van Vleck (HDV) Hamiltonian[73−75] for three ionic sites:

$$H_{HDV} = -2J_{ab}\hat{\mathbf{S}}_a \cdot \hat{\mathbf{S}}_b - 2J_{bc}\hat{\mathbf{S}}_b \cdot \hat{\mathbf{S}}_c - 2J_{ac}\hat{\mathbf{S}}_a \cdot \hat{\mathbf{S}}_c \tag{5}$$

where J_{ab} is the exchange coupling between site a and site b. A positive J_{ab} corresponds to ferromagnetic coupling (as in a high-spin diradical), and negative J_{ab} corresponds to antiferromagnetic coupling (as in singlet diradicals or half−broken covalent bonds). Just as in the previous section, we will obtain the coupling constants by carrying out electronic structure calculations (in this case described in Section 3.3.2) and fitting the resulting energies to the phenomenological Hamiltonian (in this case given by eq 5). Note that in a perfect periodic system, as is the reported experimental structure used to define the cluster,[16] J_{ab} and J_{bc} are equivalent. In the truncated model, these two interactions are not equivalent by symmetry, and hence it is crucial to extract both parameters to assess the magnitude of the deviation between these two extracted parameter values.

3.3. Electronic Structure Methods. The single-ion anisotropy is first computed using wave function approaches, allowing a multi-determinental treatment of the ligand-field states corresponding to the d^6 manifold, and therefore a consistent treatment of the ligand field and its effect on the zero-field splitting of the ground state. For the calculation of the isotropic couplings, we will use DFT, since an explicit treatment of the spin-adapted wave functions generated with three explicitly treated Fe^{II} ions would be prohibitively expensive at a very accurate level with wave function theory.

3.3.1. Methods for a Single Fe^{II} Site. We will calculate D and E by two methods, perturbation theory and a variational method.

The perturbation calculations proceed as follows. First we carry out SOC-free state-averaged complete active space self-consistent field[76] (SA-CASSCF) calculations, with averaging over either (i) the five $M_S = 0$ quintet states, which would form a degenerate ^5D state in the absence of the ligand field, or (ii) all 100 $M_S = 0$ states (five quintets, 45 triplets, and 50 singlets) arising from the d^6 configuration. Note that S is a good quantum number for the SOC-free calculations, so the singlets, triplets, and quintets form separate blocks, but they must be solved together because we want to express all states in a common set of orbitals. Then we calculate the matrix elements of the SOC operator and evaluate the elements of the $\mathbf{D}$ tensor by second-order perturbation theory applied to the ground state; the equations for this step are eqs 1−3 of ref 29, which have the form

$$D_{kl} = \sum_B \frac{\Upsilon_{kl}^{0B}}{\Delta_{0B}} \tag{6}$$

where $k,l = x,y,z$, B is an excited state with excitation energy Δ_{0B}, and γ_{kl}^{0B} is a complicated sum specified in ref 29. Next we diagonalize $\mathbf{D}$,

which yields D and E by eqs 3 and 4 above. The eigenvectors are the principal axes (magnetic axes). To see the effect of dynamical electron correlation on the perturbation theory results, we recalculate the results by replacing the SA-CASSCF values of Δ_{0B} in eq 6 by more accurate excitation energies calculated by the n-electron valence states for multireference perturbation theory[77] (NEVPT2) method.

The variational calculations[78,79] begin with an SOC-free five-state SA-CASSCF calculation. We then construct the total Hamiltonian matrix

$$\mathbf{H}_{\text{total}} = \mathbf{H}_{\text{electronic}} + \mathbf{H}_{\text{SOC}} \qquad (7)$$

in the SA-CASSCF basis, in which the SOC-free $\mathbf{H}_{\text{electronic}}$ is diagonal, and $\mathbf{H}_{\text{SOC}}$ is non-diagonal (with zeros on the diagonal) and is given by the expression of Neese under the mean-field approximation,[79] based on earlier work by Hess et al.[78] We consider only the quintet subspace, but because M_S is no longer a good quantum number we now must consider all 25 quintet states that correlate with the ^5D bare ion manifold. We diagonalize $\mathbf{H}_{\text{total}}$ and find that the five lowest states have a weight of more than 95% on the ground SOC-free state, so we are justified in considering only these states for determining D and E (under the usual assumption that the zero field splitting is smaller than the ligand field splitting).

The variational calculations with the Hamiltonian of eq 7 are carried out in the basis of the spin components of the SA-CASSCF eigenvectors, which is usually called the spin−orbit state interaction (SO-SI) method. While other approaches, such as the RASSI-SO method,[80,81] do not require using a common set of molecular orbitals, the method used here, which is the one implemented in ORCA,[82] requires an orthogonal many-electron basis, which is only achieved with a common set of orbitals for all states. One should note, however, that this requirement, rather than being a limitation, may actually be beneficial for computing the effective zero-field splitting of the ground-state spin components. Indeed, by accounting for all the spin−orbit components of the ^5D free ion manifold within the same orbital set, one ensures that the representation of the spin−orbit excitations is well balanced for all orientations of space, which is crucial for accurate computations of this anisotropic property.

The five quintet states have four energy splittings, and we could fit the four variational energy splittings of the five lowest states to the four energy spacings of Table 2 by least-squares. Instead we take a simpler approach, in particular obtaining the parameters by using the second, third, and fourth energies in Table 2. This yields

$$D = \frac{1}{3}\left\{E(\phi_2) - \frac{E(\phi_3) + E(\phi_4)}{2}\right\} \qquad (8)$$

and

$$E = \frac{1}{6}\{E(\phi_4) - E(\phi_3)\} \qquad (9)$$

The model Hamiltonian of eqs 1 and 2 does not consider any anisotropic fourth-order terms, which are nonnegligible in the case of nearly degenerate same-spin states.[47,48] Because of the highly distorted environment of the Fe^{II} ion, these terms are expected to be very small, although not strictly zero. As a consequence, a reconstructed model spectrum, obtained by using the extracted D and E parameters values, is not expected to perfectly match the set of variational energies from which they were obtained by fitting. To estimate the quality of the model spectrum, a mean percentage of error δ is computed as follows

$$\delta = \frac{\sum_{i=1}^{N}|E_i^{\text{ab initio}} - E_i^{\text{mod el}}|}{N \times \Delta E^{\text{ab initio}}} \times 100 \qquad (10)$$

where N is the number of roots, $\Delta E^{\text{ab initio}}$ is the ab initio spectrum width, and $E_i^{\text{ab initio}}$ and E_i^{model} are the ab initio and model energies, respectively. Note that in the present case, N is five.

To include dynamical electron correlation in the variational calculations, we replace the SA-CASSCF energies on the diagonal of $\mathbf{H}_{\text{electronic}}$ by NEVPT2 eigenvalues, and we repeat the procedure leading to eqs 8 and 9. Such a treatment assumes that the main dynamical correlation effect is the revision of the excitation energies while the off-diagonal SOC matrix elements are almost unchanged, and was first introduced by Llusar et al. to compute spin−orbit splittings.[83]

A smaller basis set[84] is initially considered to select a small state-interaction space, accounting for the most important contributions within the d^6 manifold. This basis set consists of the def2-SV(P) bases for all atoms (i.e., 5s3p2d1f for Fe and Zn, 3s2p1d for O and C, and 2s for H atoms). A larger basis set[84] is then used, in particular def2-TZVPP for Fe and Zn atoms (i.e., 6s5p4d2f1g), def2-TZVPP for O atoms (i.e., 5s3p2d1f), and def2-SV(P) for C and H atoms.

3.3.2. Methods for Intersite Exchange Coupling. We calculated J_{ab}, J_{bc}, and J_{ac} by Kohn−Sham DFT. We used the M06-L[85] and M06[86] exchange-correlation functionals, the def2-TZVP basis set,[84] the density fitting algorithm for Coulomb integrals to reduce computer time in M06-L calculations, and a density functional integration grid with 99 radial nodes and 590 angular nodes.

A key issue is the initial guess for orbitals to start the SCF process. We use a guess that corresponds to a local quintet on each Fe^{II} center. Then we optimize the Slater determinant by the Kohn−Sham method without any symmetry constraints and breaking all symmetries until the lowest-energy stable solution is obtained.

Although each Fe^{II} center has $|M_S| = 2$, we can arrange the centers in various combinations of spin up ($M_S = +2$) and spin down ($M_S = −2$), which generates various Slater determinants. We label the determinants corresponding to these combinations as $|M_S(a),M_S(b),M_S(c)\rangle$. Then we can obtain the exchange coupling constants from the following equations:

$$\langle 2,\, 2,\, 2|\hat{H}_{\text{HDV}}|2,\, 2,\, 2\rangle = -8J_{ab} - 8J_{bc} - 8J_{ac}$$

$$\langle -2,\, 2,\, 2|\hat{H}_{\text{HDV}}|-2,\, 2,\, 2\rangle = +8J_{ab} - 8J_{bc} + 8J_{ac}$$

$$\langle 2,\, -2,\, 2|\hat{H}_{\text{HDV}}|2,\, -2,\, 2\rangle = +8J_{ab} + 8J_{bc} - 8J_{ac}$$

$$\langle 2,\, 2,\, -2|\hat{H}_{\text{HDV}}|2,\, 2,\, -2\rangle = -8J_{ab} + 8J_{bc} + 8J_{ac} \qquad (11)$$

Solving these equations gives

$$J_{ab} = \frac{1}{32}\{E_{|2,-2,2\rangle} - E_{|2,2,2\rangle} + E_{|-2,2,2\rangle} - E_{|2,2,-2\rangle}\}$$

$$J_{bc} = \frac{1}{16}\{E_{|2,2,-2\rangle} - E_{|-2,2,2\rangle} + 16J_{ab}\}$$

$$J_{ac} = \frac{1}{16}\{E_{|2,2,-2\rangle} - E_{|2,2,2\rangle} - 16J_{bc}\} \qquad (12)$$

3.3.3. Software. All WFT calculations were carried out with the ORCA program.[82] All DFT calculations were carried out with Gaussian 09.[87]

4. RESULTS

4.1. Magnetic Data. Variable field magnetization data collected at 1.8 K reveal a sigmoidal dependence on the magnetic field, as shown in Figure 4. At zero field, the magnetization of the sample is zero, and it increases slowly with increasing H until a field strength of 1 T, when the magnetization sharply increases. At 7 T, the magnetization reaches 5.10 $N\beta$, far short of the expected 8 $N\beta$ for two isotropic $S = 2$ centers at saturation. The magnetization appears to be still increasing at these field magnitudes; thus saturation is not yet observed. Upon decreasing the field from 7 T, there is no observed hysteresis, and no remanent magnetization upon returning to 0 T. With increasing temperature, the profile of the M vs H curve loses its sigmoidal shape, approaching a Brillouin-like function[88] at 12 K, but still lacking clear magnetic saturation. We note that at the higher fields, no hysteretic behavior is observed, suggesting that the high-field phase of this material is paramagnetic in nature, rather than ferromagnetic.
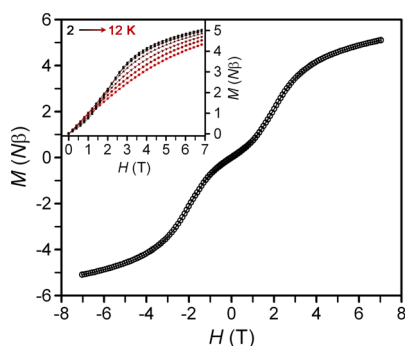
Figure 4. Variable-field (H) magnetization (M) data collected on a powder sample of $Fe_2(dobdc)$ at 1.8 K and an average field sweep rate of 2 Oe/s. The magnetization is depicted per formula unit, which includes two Fe^{II} ions. Inset: Variable temperature variable field magnetization data collected from 2 to 12 K.

The paramagnetic nature of the high-field phase is further corroborated by AC in phase (χ'_M) and out-of-phase (χ''_M) susceptibility studies, which revealed no slow magnetic relaxation at low temperature for either the low-field phase or the high-field phase (see Figures 5 and 6). At high fields,
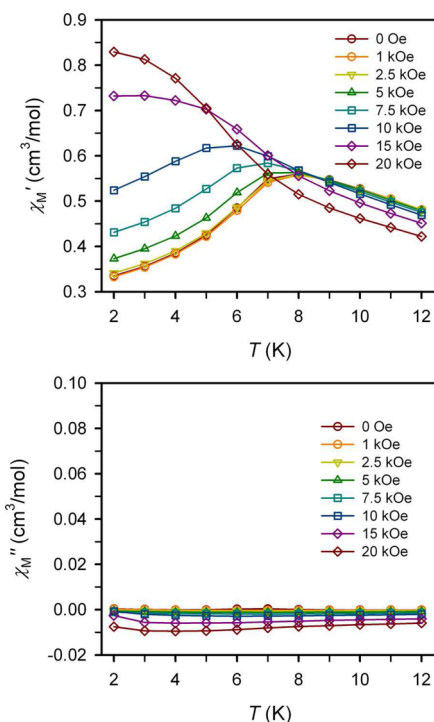
Figure 5. Variable temperature in-phase (χ'_M, top) and out-of-phase (χ''_M, bottom) AC susceptibility for $Fe_2(dobdc)$ collected at an applied AC field frequency of 10 Hz and various applied DC fields, as denoted in the figure legends.

however, the cusp in the low temperature in-phase AC susceptibility, χ'_M, appears to move to lower temperatures. Thus, the applied DC fields appear to nullify the magnetic interactions responsible for the decrease in χ'_M at low temperature.

4.2. Single-Ion Anisotropy. *4.2.1. Safe Reduction of the State-Interaction Space.* A first choice of a state-interaction space consists of all the crystal-field states belonging to the d^n manifold. For the d^6 configuration under study, this implies the
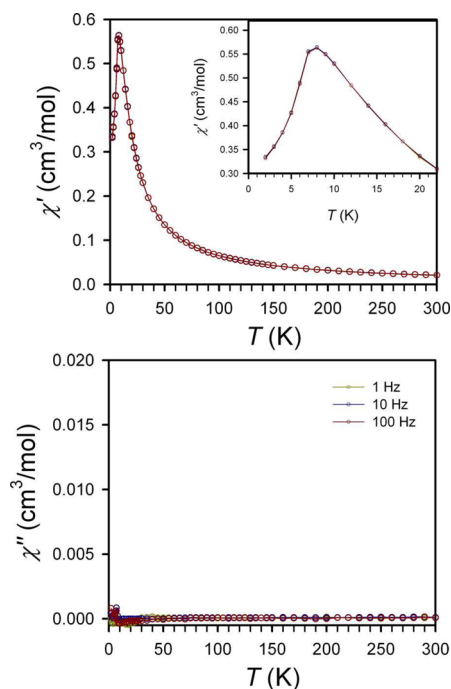
Figure 6. Variable temperature in-phase (χ'_M, top) and out-of-phase (χ''_M, bottom) AC susceptibility for $Fe_2(dobdc)$ collected at AC field frequencies of 1 (yellow), 10 (blue), and 100 (red) Hz collected at zero applied DC field. Inset: Zoom in below 20 K, highlighting the cusp in χ'_M.

computation of five quintets (Q), forty five triplets (T), and fifty singlets (S), for a total of 210 (spin−orbit) states. Such state-interaction space is naturally well balanced in all the orientations in space, which makes it adequate for the calculation of an anisotropic property. However, since SA-CASSCF calculations are performed by optimizing democratically the orbitals on all the states, the orbitals obtained may not be optimal for the description of the ground state and of the states most contributing to the single-ion anisotropy. Hence, it is wise to try to reduce the state-interaction space to a smaller set of states to better describe the dominant contributions.[34]

To choose a smaller subset of states, we first calculate the D and E parameters with all the states belonging to the d^6 manifold and second-order perturbation theory. For this large number of states, def2-SV(P) basis sets[84] are used for all atoms to reduce computational cost. As explained in Section 3.3.1, the SA-CASSCF calculations need to include only 100 of the 210 states. The SA-CASSCF excitation energies (ΔE) are presented in Table 3; the bottom row of the table gives the range of the 99 excitation energies and the final perturbation theory values of D and E. The three rows above give the range of excitation energies for all quintet excited states, all triplet, and all singlets. The last two columns of the table give the contributions of individual quintet states and the group of quintets, triplets, and singlets to D and E. These individual contributions are obtained by rotating the state contributions to the **D** tensor to the magnetic axis frame; the diagonal elements in this frame sum over states to the final D and E values, and so these diagonal elements are interpreted as the individual state contributions. From these results, it is clear that the states with lower spin multiplicity than the ground Q_1 state are much higher in energy than the same-spin (i.e., quintet) states, which indicate that $Fe_2(dobdc)$ is in a weak ligand-field regime.[89] The largest

Table 3. Excitation Energies and Contributions to the D and E Parameters Obtained at Second Order of Perturbation with the CASSCF States[a] and Energies

state(s)	ΔE (eV)	D (cm^{-1})	E (cm^{-1})
Q_2	0.12	−7.92	+2.29
Q_3	0.30	−4.84	+1.14
Q_4	0.49	−0.98	+0.86
Q_5	1.32	+0.36	−0.16
Q states	0.00−1.32	−13.38	+4.13
T states	2.10−8.52	−1.37	+0.43
S states	3.02−14.98	0.00	0.00
d^6 manifold	0.00−14.98	−14.75	+4.56

[a]The CASSCF states were obtained by a state average calculation that includes the entire d^6 manifold (see text).

contribution from a triplet state to the D parameter in absolute value is 0.55 cm^{-1}, while the sum of all the triplet state contributions accounts for less than 10% of the total D parameter value (see Table 3). Moreover, the largest individual triplet contribution to E is 0.32 cm^{-1}, while the sum of the triplet contributions give 0.43 cm^{-1}, that is, less than 10% of the total parameter value (see Table 3). As a consequence, the single-ion anisotropy is dominated by same-spin spin−orbit interactions, and the state-interaction space can be safely reduced to the quintet spin states only. Such reduction allows efficient computations at higher levels of theory, in particular, larger basis sets and post-CASSCF levels. In all the tables after Table 3 we use the larger basis set described in Section 3.3.1.

4.2.2. Role of Dynamical Correlation and the Orientation of the Magnetic Axes. To assess the role of dynamical correlation on the single-ion anisotropy, the D and E parameters were determined with second-order perturbation theory as above, but with the small state space (quintets only) and the larger basis set. Then, these results were compared to calculations employing NEVPT2 diagonal energies as explained in Section 3.3.1. The results are shown in Tables 4 and 5. These

Table 4. Excitation Energies and Contributions to the D and E Parameters Obtained at Second Order of Perturbation with the CASSCF States[a] and Energies

state(s)	ΔE (eV)	D (cm^{-1})	E (cm^{-1})
Q_2	0.12	−10.00	+1.74
Q_3	0.31	−3.60	+1.54
Q_4	0.51	−0.31	+1.09
Q_5	1.35	+0.37	−0.19
Q states	0.00−1.35	−13.54	+4.18

[a]The CASSCF states were obtained by a state average calculation that includes all five quintet states of the d^6 manifold (see text).

tables show that the use of the NEVPT2 excitation energies results in slightly lower values of the total anisotropy parameters. The ground quintet state is more stabilized by dynamical correlation than the other quintet states, which results in larger excitation energies at the NEVPT2 level for the same-spin states and weakens each individual contribution to the total anisotropy tensor.

Since the effect of the dynamical correlation on the four excited quintets is not the same, the magnetic anisotropy axes

Table 5. Excitation Energies and Contributions to the D and E Parameters Obtained at Second Order of Perturbation with the CASSCF States[a] and the NEVPT2 Excitation Energies

state(s)	ΔE (eV)	D (cm^{-1})	E (cm^{-1})
Q_2	0.14	−7.56	+1.82
Q_3	0.32	−4.24	+1.29
Q_4	0.60	−0.55	+0.79
Q_5	1.49	+0.34	−0.18
Q states	0.00−1.49	−12.01	+3.72

[a]The CASSCF states have been obtained by a state average calculation that includes all five quintet states of the d^6 manifold (see text).

are affected by the use of the NEVPT2 excitation energies, which results in larger contributions to the D and E parameters for some excited states (here larger contributions for Q_3 and Q_4 to D, and Q_2 to E). The easy axis of magnetization (here z by convention since D is negative) is moved by 3.4° by using the NEVPT2 excitation energies instead of the CASSCF ones, while the hard axis (in this case x by convention) is moved by 1.0° and the intermediate axis by 3.4°. The magnetic anisotropy axes obtained with the NEVPT2 excitation energies and second-order perturbation theory are represented in Figure 7.
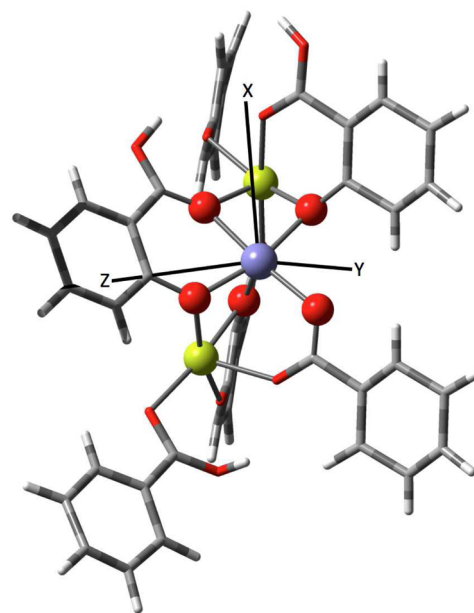
Figure 7. Modified 88-atom cluster and its magnetic anisotropy axes obtained with second-order perturbation theory with the NEVPT2 excitation energies, where the modification is the replacement of two Fe atoms by Zn atoms. The Zn atoms are represented in yellow, the Fe atom in purple, O atoms in red, C atoms in dark gray, and H atoms in light gray.

These axes do not correspond to any simple orientations defined from the first coordination sphere, for example, Fe−O orientations. Although each Fe^{II} ion is equivalent in the crystal (see Figure 1), local anisotropy axes belonging to nearest neighbors are not collinear, owing to the helical nature of the chain. As a consequence, the local anisotropy axes depicted in Figure 7 do not correspond to any easy, intermediate, or hard axes of magnetization of the crystal.

4.2.3. Extraction of the Anisotropy Parameters by Variational Calculations. The values of the anisotropy

parameters discussed so far were determined from second-order perturbation theory. To check if second-order perturbation theory is a good approximation in this case, the anisotropy parameters are also extracted by a variational method. However, as described in Section 3.3.1, the variational and model energies may not perfectly match in this case since the spin–allowed fourth-order terms are neglected in the model Hamiltonian. As a consequence, there is no unique way of extracting directly the D and E parameter values from the ab initio energies, but we extract them by a straightforward scheme described in Section 3.3.1. As shown in Table 6, the resulting

Table 6. D and E Parameter Values (in cm^{-1}) Extracted from the Ab Initio Energies as Functions of the Energies Used on the Diagonal Elements of the SOC Matrix

parameter	CASSCF	NEVPT2
D	−11.93	−10.87
E	+3.40	+3.17

values are very close to the ones obtained with second-order perturbation theory (see Tables 4 and 5), validating the use of perturbation theory for determining the D and E parameters in this system.

To validate a posteriori the neglect of the fourth-order terms in the model Hamiltonian, the ab initio and reconstructed model spectrum are compared (see Tables 7 and 8). The ϕ_i

Table 7. Ab Initio and Model Reconstructed Spectrum ($\hat{H}_{mod} = D\hat{S}_z^2 + E[\hat{S}_x^2 - \hat{S}_y^2]$), Where the Ab Initio Spectrum Has Been Obtained Using the CASSCF States and Energies

state	$E^{ab\ initio}$ (cm^{-1})	E^{model} (cm^{-1})	model vectors
ϕ_1	−2.50	−2.75	$\approx \frac{1}{\sqrt{2}}[\lvert2,2\rangle + \lvert2,-2\rangle]$
ϕ_2	0.00	0.00	$\frac{1}{\sqrt{2}}[\lvert2,2\rangle - \lvert2,-2\rangle]$
ϕ_3	25.57	25.57	$\frac{1}{\sqrt{2}}[\lvert2,1\rangle - \lvert2,-1\rangle]$
ϕ_4	45.99	45.99	$\frac{1}{\sqrt{2}}[\lvert2,1\rangle + \lvert2,-1\rangle]$
ϕ_5	50.80	50.46	$\approx\lvert2,0\rangle$

Table 8. Ab Initio and Model Reconstructed Spectrum ($\hat{H}_{mod} = D\hat{S}_z^2 + E[\hat{S}_x^2 - \hat{S}_y^2]$), Where the Ab Initio Spectrum Has Been Obtained Using the CASSCF States and the NEVPT2 Excitation Energies

state	$E^{ab\ initio}$ (cm^{-1})	E^{model} (cm^{-1})	model vectors
ϕ_1	−2.42	−2.62	$\approx \frac{1}{\sqrt{2}}[\lvert2,2\rangle + \lvert2,-2\rangle]$
ϕ_2	0.00	0.00	$\frac{1}{\sqrt{2}}[\lvert2,2\rangle - \lvert2,-2\rangle]$
ϕ_3	23.10	23.10	$\frac{1}{\sqrt{2}}[\lvert2,1\rangle - \lvert2,-1\rangle]$
ϕ_4	42.13	42.13	$\frac{1}{\sqrt{2}}[\lvert2,1\rangle + \lvert2,-1\rangle]$
ϕ_5	46.30	46.10	$\approx\lvert2,0\rangle$

states correspond to either the computed spin–orbit states or the model states, belonging to the ab initio and model reconstructed spectrum, respectively. The ϕ_2 state is chosen as

the zero of the energy since it is perfectly described according to the extraction scheme utilized (see Section 3.3.1). With this extraction scheme, the ϕ_3 and ϕ_4 model energies also perfectly match the variational ones, and then the mismatch between the spectra is relegated to ϕ_1 and ϕ_5. As can be seen, the model and variational energies match fairly well for both states at both levels of theory, and this results in a small error δ according to eq 10 (0.23% with the CASSCF excitation energies and 0.16% with the NEVPT2 ones). As a consequence, it is concluded that the fourth-order terms can be neglected in the model Hamiltonian to extract the second-order anisotropy parameters, that is, the D and E parameters. One should note that the order of the operators used in the model Hamiltonian is distinct from the order of operators used in the Hamiltonian of eq 7. For instance, since the parameters extracted from the variational energies differ slightly from the ones obtained with second-order perturbation theory, higher-order SOC effects affect the computed D and E parameter values.

4.3. Isotropic Couplings. The relative energies of the four possible combinations of ferromagnetic or antiferromagnetic coupling of the three Fe^{II} quintet centers obtained with the M06-L and M06 exchange-correlation functionals are given in Table 9. Note that in a periodic treatment of the MOF crystal,

Table 9. Relative Energies of Selected Spin Broken-Symmetry Solutions, Obtained Using the M06-L and M06 Exchange-Correlation Functionals

	E (cm^{-1})	
$\lvert M_S(a), M_S(b), M_S(c)\rangle$	M06-L	M06
$\lvert2,2,2\rangle$	0.00	0.00
$\lvert-2,2,2\rangle$	222.83	97.49
$\lvert2,-2,2\rangle$	330.17	115.58
$\lvert2,2,-2\rangle$	170.70	34.89

$\lvert-2,2,2\rangle$ and $\lvert2,2,-2\rangle$ would be the same but in the 88-atom model they are slightly different. Table 10 shows the resulting

Table 10. Isotropic Magnetic Couplings J_{ab}, J_{bc}, and J_{ac} Obtained with the M06-L and M06 Exchange-Correlation Functionals

|	value (cm^{-1})	
parameter	M06-L	M06
J_{ab}	+11.9	+5.6
J_{bc}	+8.7	+1.7
J_{ac}	+2.0	+0.5

exchange couplings obtained by eqs 11 and 12. Since J_{ab} differs from J_{bc} only because of truncation of the periodic crystal to 88 atoms, we may average them to obtain a nearest-neighbor (NN) coupling constant of J_{NN} = 10.3 cm^{-1} at the M06-L level, which may be compared to the next-nearest-neighbor (NNN) value of J_{NNN} = 2.0 cm^{-1}, while at the M06 level values of J_{NN} = 3.6 cm^{-1} and J_{NNN} = 0.5 cm^{-1} are obtained. Given the small magnitude of J_{NNN}, its ferromagnetic or antiferromagnetic nature cannot be unequivocally determined, but since both exchange-correlation functionals led to ferromagnetic NNN couplings, we conclude that these interactions are probably ferromagnetic, although small. Note that with both the NN and NNN interactions within a chain being ferromagnetic, no frustration would be expected within the chains. A value of J_{NN} = 4.1 cm^{-1} was obtained experimentally,[2] and periodic

calculations with a different functional also led to ferromagnetic J_{NN} and J_{NNN} couplings, with larger values than in the present work.[26] We conclude that both experiment and theory suggest that the NN interactions are ferromagnetic but small.

5. DISCUSSION

Each Fe^{II} ion in the crystal has a pentacoordinate environment in its first coordination sphere. With a perfect SPy geometry and in the absence of SOC, the ground state would be an orbital doublet, that is, two orbital configurations would be degenerate. In an atomic orbital picture of the ligand field, such situation would correspond to a degeneracy between two d orbitals of the transition metal ion (see Figure 8). In this
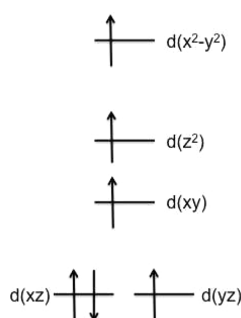
Figure 8. Splitting of the Fe^{2+} d orbitals under a SPy ligand field. Note that the labeling of the orbitals depends on the coordinate frame and on the ligand field strength. Electrons are displayed to illustrate one of the two degenerate high-spin configurations.

situation, the model space would have 10 components, the 5 spin components associated with each of the 2 degenerate orbital configurations. However, the first coordination sphere of the Fe^{II} ions is distorted, and further deviations from the ideal geometry are also related to the presence of other Fe^{II} ions in the second coordination sphere, and longer range crystalline anisotropy. As a consequence, the ground state is an orbital singlet, that is, it is non-degenerate, and the degeneracy of the (ground) quintet spin components is lifted because of the anisotropy of the ligand field and SOC, which has been effectively described in the present study by using a simple spin Hamiltonian approach accounting for only the five spin components of this ground (orbital) state. The weak ligand field imposed by the $dobdc^{4-}$ ligands results in small same-spin excitation energies and therefore the single-ion anisotropy is very large in this anisotropic system.

The single-ion anisotropy is large compared to the nearest neighbor isotropic magnetic couplings. This classifies the system as being in the weak-exchange regime.[90] Since the local anisotropy axes of the Fe^{II} ions are not collinear, the macroscopic behavior cannot be predicted from this local information. As pointed out in Section 3.2, negative D can lead to permanent magnetization; however, it is not sufficient, especially if it is small. We find that D is negative and quite large. It is however probable that the mismatch between single-ion anisotropies and the weak-exchange regime opens the way for fast relaxation pathways for the macroscopic magnetization, so $Fe_2(dobdc)$ is not expected to behave as a magnet. This is consistent with experiment, since no slow magnetic relaxation is visible in the out-of-phase AC susceptibility under zero applied DC field (see Figures 5 and 6), nor is there any observed

hysteresis in the magnetization vs field curves at temperatures down to 2 K.

Another interesting feature of the M vs H curve is the sigmoidal shape observed at low temperature, indicating a metamagnetic behavior. This type of behavior is compatible with previous fits of the susceptibility data, which incorporated ferromagnetic chains with weak antiferromagnetic interchain interactions,[2] since the presence of these interchain interactions can explain such behavior.[61] In the field dependence of the in-phase AC susceptibility data (see Figure 5), the cusp, suggestive of freezing the magnetic or metamagnetic interactions, appears to be eliminated under increasingly higher DC magnetic fields. Alternatively, the combination of a weak-exchange regime and noncollinear single-ion anisotropy could also cause an abrupt change in the magnetization vs field curve at low temperature. Indeed, in such situations, the lowest-lying spin—orbit levels would show strong mixtures of different local spin configurations. By increasing the field, the spin—orbit levels would be dramatically affected, resulting in a higher spin angular momentum in the ground level, and thus in a higher magnetization. Unfortunately, it would be a difficult task to model the complexity of such a situation, and, to the best of our knowledge, no program is able to properly model the complexity of this situation (weak exchange plus noncollinear anisotropies), although recent efforts for a 1D-exchange coupled system with noncollinear single-ion anisotropies are worth noting.[91]

Other intersite effective interactions, such as antisymmetric exchange (often referred as the Dzyaloshinskii—Moriya interaction),[92,93] biquadratic antisymmetric exchange,[94] symmetric exchange,[93] biquadratic symmetric exchange,[95] or even higher-rank anisotropic terms are spatial- and spin-symmetry allowed in $Fe_2(dobdc)$. As shown in the literature,[93,96,97] antisymmetric interactions can be observed if the magnetic centers are "connected" via anisotropic superexchange[98] interactions. Symmetric exchange terms require nonzero isotropic magnetic couplings in excited states for which one electron is promoted to a combination of local ligand-field excited states.[71] Since in $Fe_2(dobdc)$ the single-ion anisotropy is found to be very large, and since the magnetic centers are not strongly coupled, intersite anisotropic terms are expected to have a weaker influence on the magnetism of this system than the single-ion anisotropy, and therefore they were not considered in the present study. One should note, however, that these interactions may also play an important role at low temperature, as may any nonzero effective interaction present in the sample.

6. CONCLUDING REMARKS

The further development of the utility of $Fe_2(dobdc)$ requires a thorough understanding of the properties of the material. First and foremost, insight into the electronic structure of the compound may reveal design principles for future MOFs with improved properties. The model presented here addresses the influence of the anisotropy of the high-spin Fe^{II} centers, as well as the magnetic couplings between them, on the magnetic properties of $Fe_2(dobdc)$. Importantly, while information about the anisotropy cannot be obtained in a straightforward way from experiment because of the mismatch between the local axes belonging to nearest and next-nearest neighbors, the electronic structure calculations can make efficient and accurate predictions within the cluster approach.

The isotropic couplings between the nearest and next-nearest neighbors, also computed within the same framework, confirm, in agreement with the experimental findings, that the most important coupling in Fe_2(dobdc) is the ferromagnetic nearest neighbor interaction, and also show, to a lesser extent, next-nearest neighbor ferromagnetic interactions. However, the relative magnitude of the computed single-ion anisotropy places this system in the weak-exchange regime. Further, the noncollinear Fe^{II} single-ion anisotropies will partially cancel out when averaged over the crystallite. These considerations provide a reasonable explanation of the lack of an observation of bulk magnetic properties attributable to magnetocrystalline anisotropy.

Fast magnetic relaxation is demonstrated for Fe_2(dobdc), as evidenced in the featureless out-of-phase AC susceptibility data as well as the absence of hysteresis in the magnetization vs field curves down to 2 K. At low temperatures, a sigmoidal shape is observed in these curves, evidencing a metamagnetic behavior. It is hard to know at this stage which effective interactions are most responsible for the absence of hysteresis (i.e., responsible for effectively instantaneous relaxation of the magnetization), and which one is most responsible for the metamagnetic behavior (i.e., responsible for causing dramatic changes of the spin configuration of the ground state at moderate field values). Models and programs properly accounting for the complexity of the situation encountered in Fe_2(dobdc) and allowing one to simulate magnetization vs field curves, which would be a reasonable step for further understanding such magnetic data, have yet to be developed.

MOFs presenting magnetic centers with large single-ion anisotropies may lead to very interesting magnetic properties. However, to limit relaxation pathways for the magnetization, it would appear more attractive to study and design MOFs with collinear single-ion magnetic anisotropy axes. Given the high number of possibilities that can be generated by combining various metal-based building blocks and organic linkers, there are numerous possibilities for new magnets that may be synthesized in the near future.

■ ASSOCIATED CONTENT

Ⓢ Supporting Information

Coordinates of the 88-atom model used in the calculations of the single-ion anisotropy and of the isotropic couplings. Total energies of the broken-spin-symmetry solutions used to extract the isotropic couplings. This material is available free of charge via the Internet at http://pubs.acs.org.

■ AUTHOR INFORMATION

Corresponding Author

*E-mail: jrlong@berkeley.edu (J.R.L.), truhlar@umn.edu (D.G.T.), gagliard@umn.edu (L.G.).

Notes

The authors declare no competing financial interest.

■ ACKNOWLEDGMENTS

■ REFERENCES

(1) Leclerc, H.; Vimont, A.; Lavalley, J.-C.; Daturi, M.; Wiersum, A. D.; Llwellyn, P. L.; Horcajada, P.; Férey, G.; Serre, C. *Phys. Chem. Chem. Phys.* **2011**, *13*, 11748−11756.

(2) Bloch, E. D.; Queen, W. L.; Krishna, R.; Zadrozny, J. M.; Brown, C. M.; Long, J. R. *Science* **2012**, *335*, 1606−1610.

(3) Bae, Y.-S.; Lee, C. Y.; Kim, K. C.; Farha, O. K.; Nickias, P.; Hupp, J. T.; Nguyen, S. T.; Snurr, R. Q. *Angew. Chem., Int. Ed.* **2012**, *51*, 1857−1860.

(4) Sumida, K.; Rogow, D. L.; Mason, J. A.; McDonald, T. M.; Bloch, E. D.; Herm, Z. R.; Bae, T.-H.; Long, J. R. *Chem. Rev.* **2012**, *112*, 724−781.

(5) Li, J.-R.; Sculley, J.; Zhou, H.-C. *Chem. Rev.* **2012**, *112*, 869−932.

(6) Wu, H.; Gong, Q.; Olson, D. H.; Li, J. *Chem. Rev.* **2012**, *112*, 836−868.

(7) Lee, J.; Farha, O. K.; Roberts, J.; Scheidt, K. A.; Nguyen, S. T.; Hupp, J. T. *Chem. Soc. Rev.* **2009**, *38*, 1450−1459.

(8) Ma, L.; Abney, C.; Lin, W. *Chem. Soc. Rev.* **2009**, *38*, 1248−1256.

(9) Kurmoo, M. *Chem. Soc. Rev.* **2009**, *38*, 1353−1379.

(10) Roques, N.; Mugnaini, V.; Veciana, J. *Top. Curr. Chem.* **2009**, *293*, 207−258.

(11) Dechambenoit, P.; Long, J. R. *Chem. Soc. Rev.* **2011**, *40*, 3249−3265.

(12) Bartolomé, E.; Javier Alonso, P.; Arauzo, A.; Luzón, J.; Bartolomé, J.; Racles, C.; Turta, C. *Dalton Trans.* **2012**, *41*, 10382−10389.

(13) Senchyk, G. A.; Lysenko, A. B.; Rusanov, E. B.; Chernega, A. N.; Jezierska, J.; Domasevitch, K. V.; Ozarowski, A. *Eur. J. Inorg. Chem.* **2012**, 5802−5813.

(14) He, Y.; Krishna, R.; Chen, B. *Energy Environ. Sci.* **2012**, *5*, 9107−9120.

(15) Geier, S. J.; Mason, J. A.; Bloch, E. D.; Queen, W. L.; Hudson, M. R.; Brown, C. M.; Long, J. R. *Chem. Sci.* **2013**, *4*, 2054−2061.

(16) Bloch, E. D.; Murray, L. J.; Queen, W. L.; Chavan, S.; Maximoff, S. N.; Bigi, J. P.; Krishna, R.; Peterson, V. K.; Grandjean, F.; Long, G. J.; Smit, B.; Bordiga, S.; Brown, C. M.; Long, J. R. *J. Am. Chem. Soc.* **2011**, *133*, 14814−14822.

(17) McWeeny, R. *J. Chem. Phys.* **1963**, *42*, 1717−1725.

(18) Carrington, A.; McLachlan, A. D. *Introduction to magnetic resonance with applications to chemistry and chemical physics*; Harper and Row: New York, 1967.

(19) Freedman, D. E.; Harman, W. H.; Harris, T. D.; Long, G. J.; Chang, C. J.; Long, J. R. *J. Am. Chem. Soc.* **2010**, *132*, 1224−1225.

(20) Harman, W. H.; Harris, T. D.; Freedman, D. E.; Fong, H.; Chang, A.; Rinehart, J. D.; Ozarowski, A.; Sougrati, M. T.; Grandjean, F.; Long, G. J.; Long, J. R.; Chang, C. J. *J. Am. Chem. Soc.* **2010**, *132*, 18115−18126.

(21) Venkatakrishnan, T. S.; Shaon, S.; Bréfuel, N.; Duhayon, C.; Paulsen, C.; Barra, A.-L.; Ramasesha, S.; Sutter, J.-P. *J. Am. Chem. Soc.* **2010**, *132*, 6047−6056.

(22) Zadrozny, J. M.; Atanasov, M.; Bryan, A. M.; Lin, C.-Y.; Rekken, B. K.; Power, P. P.; Neese, F.; Long, J. R. *Chem. Sci.* **2013**, *4*, 125−138.

(23) Atanasov, M.; Zadrozny, J. M.; Long, J. R.; Neese, F. *Chem. Sci.* **2013**, *4*, 139−156.

(24) Pradipto, A.-M.; Maurice, R.; Guihéry, N.; de Graaf, C.; Broer, R. *Phys. Rev. B* **2012**, *85*, 014409.

(25) Maurice, R.; Pradipto, A.-M.; de Graaf, C.; Broer, R. *Phys. Rev. B* **2012**, *86*, 024411.

(26) Canepa, P.; Chabal, Y. J.; Thonhauser, T. *Phys. Rev. B* **2013**, *87*, 094407.

(27) Pederson, M. R.; Khanna, S. N. *Phys. Rev. B* **1999**, *60*, 9566−9572.

(28) Aquino, F.; Rodriguez, J. H. *J. Chem. Phys.* **2005**, *123*, 204902.

(29) Neese, F. *J. Am. Chem. Soc.* **2006**, *128*, 10213−10222.

(30) Neese, F. *J. Chem. Phys.* **2007**, *127*, 164112.

(31) Schmitt, S.; Jost, P.; van Wüllen, C. *J. Chem. Phys.* **2011**, *134*, 194113.

(32) Ganyushin, D.; Neese, F. *J. Chem. Phys.* **2006**, *125*, 024103.

(33) de Graaf, C.; Sousa, C. *Int. J. Quantum Chem.* **2006**, *106*, 2470−2478.

(34) Maurice, R.; Bastardis, R.; de Graaf, C.; Suaud, N.; Mallah, T.; Guihéry, N. *J. Chem. Theory Comput.* **2009**, *5*, 2977−2984.

(35) Sugisaki, K.; Toyota, K.; Sato, K.; Shiomi, D.; Kitagawa, M.; Takui, T. *Chem. Phys. Lett.* **2009**, *477*, 369−373.

(36) Chibotaru, L. F.; Ungur, L. *J. Chem. Phys.* **2012**, *137*, 064112.

(37) Vancoillie, S.; Pierloot, K. *J. Phys. Chem. A* **2008**, *112*, 4011−4019.

(38) Chibotaru, L.; Ungur, L.; Aronica, C.; Elmoll, H.; Pilet, G.; Luneau, D. *J. Am. Chem. Soc.* **2008**, *130*, 12445−12455.

(39) Chibotaru, L.; Ungur, L.; Soncini, A. *Angew. Chem., Int. Ed.* **2008**, *47*, 4126−4129.

(40) Maurice, R.; Vendier, L.; Costes, J.-P. *Inorg. Chem.* **2011**, *50*, 11075−11081.

(41) Telser, J.; Ozarowski, A.; Krystek, J. *Electron Paramagn. Reson.* **2013**, 209−263.

(42) Costes, J.-P.; Maurice, R.; Vendier, L. *Chem.—Eur. J.* **2012**, *18*, 4031−4040.

(43) Ruamps, R.; Batchelor, L. J.; Maurice, R.; Gogoi, N.; Jiménez-Lozano, P.; Guihéry, N.; de Graaf, C.; Barra, A.-L.; Sutter, J.-P.; Mallah, T. *Chem.—Eur. J.* **2013**, *19*, 950−956.

(44) Ruamps, R.; Maurice, R.; Batchelor, L. J.; Boggio-Pasqua, M.; Guillot, R.; Barra, A.-L.; Liu, J.; Bendeif, E.-E.; Pillet, S.; Hill, S.; Mallah, T.; Guihéry, N. *J. Am. Chem. Soc.* **2013**, *135*, 3017−3026.

(45) Abragam, A.; Bleaney, B. *Electron paramagnetic resonance of transition ions*; Dover Publications: Dover, NY, 1986.

(46) Telser, J. *J. Braz. Chem. Soc.* **2006**, 1501−1515.

(47) Maurice, R.; de Graaf, C.; Guihéry, N. *J. Chem. Phys.* **2010**, *133*, 084307.

(48) Atanasov, M.; Ganyushin, D.; Pantazis, D. A.; Sivalingam, K.; Neese, F. *Inorg. Chem.* **2011**, *50*, 7460−7477.

(49) McGarvey, B.; Telser, J. *Inorg. Chem.* **2012**, *51*, 6000−6010.

(50) Duboc, C.; Ganyushin, D.; Sivalingam, K.; Collomb, M.-N.; Neese, F. *J. Phys. Chem. A* **2010**, *114*, 10750−10758.

(51) Kubika, A.; Kowalewski, J.; Kruk, D.; Odelius, M. *J. Chem. Phys.* **2013**, *138*, 064304.

(52) de, P. R.; Moreira, I.; Illas, F. *Phys. Chem. Chem. Phys.* **2006**, *8*, 1645−1659.

(53) Calzado, C. J.; Cabrero, J.; Malrieu, J. P.; Caballol, R. *J. Chem. Phys.* **2002**, *116*, 2728.

(54) Calzado, C. J.; Cabrero, J.; Malrieu, J. P.; Caballol, R. *J. Chem. Phys.* **2002**, *116*, 3985.

(55) Calzado, C. J.; Angeli, C.; Taratiel, D.; Caballol, R.; Malrieu, J.-P. *J. Chem. Phys.* **2009**, *131*, 044327.

(56) Valero, R.; Costa, R.; de P. R. Moreira, I.; Truhlar, D. G.; Illas, F. *J. Chem. Phys.* **2008**, *128*, 114103.

(57) Rivero, P.; de P. R. Moreira, I.; Illas, F.; Scuseria, G. E. *J. Chem. Phys.* **2008**, *129*, 184110.

(58) Brain, G. A.; Berry, J. F. *J. Chem. Educ.* **2008**, *85*, 532.

(59) Verma, P.; Xu, X.; Truhlar, D. G. *J. Phys. Chem. C* **2013**, *117*, 12648−12660.

(60) Bogdanov, N. A.; Maurice, R.; Rousochatsakis, I.; van ben Brink, J.; Hozoi, L. *Phys. Rev. Lett.* **2013**, *110*, 127206.

(61) Wynn, C. M.; Gîrtu, M. A.; Brinckerhoof, W. B.; Suguira, K.-I.; Miller, J. S.; Epstein, A. J. *Chem. Mater.* **1997**, *9*, 2156−2163.

(62) Kar, P.; Biswas, R.; Drew, M. G. B.; Ida, Y.; Ishida, T.; Ghosh, A. *Dalton Trans.* **2011**, *40*, 3295−3304.

(63) Oprea, C. I.; Panait, P.; Cimpoesu, F.; Humelnicu, I.; Ferbinteanu, M.; Gîrţu, M. A. *Theor. Chem. Acc.* **2012**, *131*, 1249.

(64) Van Vleck, J. H. *Rev. Mod. Phys.* **1951**, *23*, 213−227.

(65) McLachlan, A. D. *Mol. Phys.* **1963**, *6*, 441−444.

(66) Abragam, A.; Pryce, M. H. L. *Proc. Roy. Soc. London Ser. A* **1951**, *206*, 135−153.

(67) Neese, F.; Solomon, E. I. *Inorg. Chem.* **1998**, *37*, 6568−6582.

(68) Gatteschi, D.; Sessoli, R. *Angew. Chem., Int. Ed.* **2003**, *42*, 268−297.

(69) Zein, S.; Duboc, C.; Lubitz, W.; Neese, F. *Inorg. Chem.* **2008**, *47*, 134−142.

(70) Zein, S.; Neese, F. *J. Phys. Chem. A* **2008**, *112*, 7976−7983.

(71) Maurice, R.; Sivalingam, K.; Ganyushin, D.; Guihéry, N.; de Graaf, C.; Neese, F. *Inorg. Chem.* **2011**, *50*, 6229−6236.

(72) Hendrich, M. P.; de Brunner, P. G. *Biophys. J.* **1989**, *56*, 489−506.

(73) Heisenberg, W. *Z. Phys* **1928**, *49*, 619−636.

(74) Dirac, P. A. M. *Proc. Roy. Soc. Lond.* **1929**, *A123*, 714−733.

(75) Van Vleck, J. H. *Rev. Mod. Phys.* **1945**, *17*, 27−47.

(76) Roos, B. O. In *Theory and applications of computational chemistry: The first forty years*; Dykstra, C. E., Frenking, G., Kim, K. S., Scuseria, G. E., Eds.; Elsevier:Amsterdam, The Netherlands, 2005; pp 725−764.

(77) Angeli, C.; Cimiraglia, R.; Evangelisti, S.; Leininger, T.; Malrieu, J.-P. *J. Chem. Phys.* **2001**, *114*, 10252−10264.

(78) Hess, B. A.; Marian, C. M.; Wahlgren, U.; Gropen, O. *Chem. Phys. Lett.* **1996**, *251*, 365−371.

(79) Neese, F. *J. Chem. Phys.* **2005**, *122*, 034107.

(80) Malmqvist, P.-Å.; Roos, B. O.; Schimmelpfennig, B. *Chem. Phys. Lett.* **2002**, *357*, 230−240.

(81) Roos, B. O.; Malmqvist, P.-Å. *Phys. Chem. Chem. Phys.* **2004**, *6*, 2919−2927.

(82) Neese, F. *ORCA, An ab initio, density functional and semiempirical program package*, Version 2.9; Max Planck Institut für Bioanorganische Chemie: Mülheim an der Ruhr, Germany, 2012.

(83) Llusar, R.; Casarrubios, M.; Barandiarán, Z.; Seijo, L. *J. Chem. Phys.* **1996**, *105*, 5321−5330.

(84) Weigend, F.; Ahlrichs, R. *Phys. Chem. Chem. Phys.* **2005**, *7*, 3297−3305.

(85) Zhao, Y.; Truhlar, D. G. *J. Chem. Phys.* **2006**, *125*, 194101.

(86) Zhao, Y.; Truhlar, D. G. *Theor. Chem. Acc.* **2008**, *120*, 215−241.

(87) Frisch, M. J.; Trucks, G. W.; Schlegel, H. B.; Scuseria, G. E.; Robb, M. A.; Cheeseman, J. R.; Scalmani, G.; Barone, V.; Mennucci, B.; Petersson, G. A.; Nakatsuji, H.; Caricato, M.; Li, X.; Hratchian, H. P.; Izmaylov, A. F.; Bloino, J.; Zheng, G.; Sonnenberg, J. L.; Hada, M.; Ehara, M.; Toyota, K.; Fukuda, R.; Hasegawa, J.; Ishida, M.; Nakajima, T.; Honda, Y.; Kitao, O.; Nakai, H.; Vreven, T.; Montgomery, J. A., Jr.; Peralta, J. E.; Ogliaro, F.; Bearpark, M.; Heyd, J. J.; Brothers, E.; Kudin, K. N.; Staroverov, V. N.; Kobayashi, R.; Normand, J.; Raghavachari, K.; Rendell, A.; Burant, J. C.; Iyengar, S. S.; Tomasi, J.; Cossi, M.; Rega, N.; Millam, J. M.; Klene, M.; Knox, J. E.; Cross, J. B.; Bakken, V.; Adamo, C.; Jaramillo, J.; Gomperts, R.; Stratmann, R. E.; Yazyev, O.; Austin, A. J.; Cammi, R.; Pomelli, C.; Ochterski, J. W.; Martin, R. L.; Morokuma, K.; Zakrzewski, V. G.; Voth, G. A.; Salvador, P.; Dannenberg, J. J.; Dapprich, S.; Daniels, A. D.; Farkas, Ö.; Foresman, J. B.; Ortiz, J. V.; Cioslowski, J.; Fox, D. J. *Gaussian 09*, Revision C.01; Gaussian Inc.: Wallingford, CT, 2009.

(88) Boča, R. *Coord. Chem. Rev.* **2004**, *248*, 757−815.

(89) Yamamoto, A. *Organotransition Metal Chemistry*; Wiley: New York, 1986.

(90) Boča, R. *Theoretical foundations of molecular magnetism*; Elsevier: Amsterdam, The Netherlands, 1999.

(91) Sahoo, S.; Sutter, J.-P.; Ramasesha, S. *J. Stat. Phys.* **2012**, *147*, 181−193.

(92) Dzyaloshinskii, I. *J. Phys. Chem. Solids* **1958**, *4*, 241−255.

(93) Moriya, T. *Phys. Rev.* **1960**, *120*, 91−98.

(94) Plumer, M. L. *Phys. Rev. B* **2007**, *76*, 144411.

(95) Maurice, R.; Guihéry, N.; Bastardis, R.; de Graaf, C. *J. Chem. Theory Comput.* **2010**, *6*, 55−65.

(96) Moskvin, A. S. *J. Exp. Theor. Phys.* **2007**, *104*, 913−927.

(97) Maurice, R.; Pradipto, A. M.; Guihéry, N.; Broer, R.; de Graaf, C. *J. Chem. Theory Comput.* **2010**, *6*, 3092−3101.

(98) Anderson, P. W. *Phys. Rev.* **1950**, *79*, 350−356.